Quantum Mechanical Capture/Phase Space Theory Calculation of the Rate Constants for the Complex-Forming CH + H_2 Reaction

Amaia Saracibar,[†,‡] Evelyn M. Goldfield,[*,†] and Stephen K. Gray[§]

Department of Chemistry, Wayne State University, Detroit, Michigan 48202, Departamento de Química Física, Universidad del País Vasco 01006, Vitoria, Spain, and Chemical Sciences and Engineering Division, Argonne National Laboratory, Argonne, Illinois 60439

Received: July 3, 2008; Revised Manuscript Received: September 15, 2008

Six-dimensional wave packet calculations on an accurate potential energy surface are used to obtain the quantum mechanical capture (QM C) probabilities for CH + H_2 corresponding to a variety of total angular momenta and internal reactant states. Rate constant calculations are made feasible by employing a Monte Carlo based sampling procedure. The QM C probabilities alone are also used to estimate the high pressure CH + H_2 rate constants corresponding to stabilization or CH_3 formation. The rate constants for CH + H_2 → CH_2 + H reaction in the low pressure limit are obtained by combining the QM C probabilities with a phase space theory (PST) approximation for product formation from the complex. Our results are compared with the experimental results of Brownsword et al. (*J. Chem. Phys.* **1997**, *106*, 7662), as well as with purely classical PST calculations. The QM C probabilities are shown to be highly dependent on the initial rotational states of the reactants corresponding to orientational restrictions on complex formation. Consistent with this, our QM C high pressure rate constants for CH_3 formation are lower than the purely classical PST rate constants. These QM C rate constants also are in reasonable accord with experiment. A similar but somewhat more subtle picture emerges regarding the QM C/PST rate constants for CH_2 + H formation.

I. Introduction

The gas phase reaction system:

$$\mathrm{CH}(^2\Pi) + \mathrm{H_2} \rightarrow \mathrm{CH_3^*} \rightarrow \mathrm{CH_2}(\mathrm{X}^3\mathrm{B_1}) + \mathrm{H} \qquad \text{(R1)}$$

$$\downarrow [M]$$

$$\mathrm{CH_3} \qquad \text{(R2)}$$

is interesting from several perspectives. First, it is one of the simplest systems involving the methylidene radical, CH, a highly reactive species of relevance to combustion chemistry. Second, it involves intermediate methyl radical CH_3* (X^2A_2'') complexes, making it a good test case for understanding the role of complexes in bimolecular chemical reactions. Finally, the minimum energy path for CH_3* formation is somewhat unusual in that the two diatomic reactants are oriented parallel to one another as they approach, and only at a surprisingly short separation of their centers of mass (∼2.5 au) do they adopt the more intuitive C_{2v} insertion path.[1−3] Consequently, there have been numerous experimental and theoretical studies of this system.[1−9] Reaction (R1) is a barrierless, endothermic reaction with $\Delta H_0(0\ \mathrm{K}) = 0.145 \pm 0.006$ eV, whereas $\Delta H_0(0\ \mathrm{K}) = -4.592 \pm 0.003$ eV for (R2).[3]

In a previous work[3] (hereafter, Paper I), we carried out quasiclassical trajectory (QCT) and quantum wavepacket calculations on the forward reaction (R1) consistent with the low ("zero") pressure gas phase limit where (R2) is not relevant. These calculations used a global potential energy surface that incorporated very high level ab initio electronic structure information.[10] Severe zero-point energy violation was found to occur in the classical trajectories, leading to a flat, near gas-kinetic QCT-based rate constant of $\sim 4 \times 10^{-11}$ cm^3 molec^{-1}s^{-1} in the 300−1000 K temperature range. In contrast, experimental measurements of the low pressure rate constant[5] vary from $\sim 3 \times 10^{-12}$ cm^3 molec^{-1}s^{-1} to $\sim 3 \times 10^{-11}$ cm^3 molec^{-1}s^{-1} across this temperature range, i.e., only agree with the QCT result in the high temperature limit. The quantum calculations were limited to total angular momentum, $J = 0$, thus not permitting a reliable estimate of the full rate constant. However, we were able to validate a quantum mechanical capture/phase space theory (QM C/PST) model for approximating the quantum reaction probabilities, wherein the reaction probability is equated with a product of a quantum mechanical capture (QM C) probability and a phase space theory (PST) probability for product formation. Our use of such capture-based quantum mechanical ideas was motivated by the earlier capture-based wave packet work of Lin and Guo[11,12] and time-independent scattering work of Manolopoulos and co-workers.[13] A statistical quasiclassical trajectory method has also been developed by Aoiz and co-workers.[14] While not involving capture ideas, we note also the statistical sampling approach of Matzkies and Manthe[15] which allows the direct, quantum mechanical calculation of thermal rate constants. In finite pressure experiments, the loss of CH + H_2 is due to a competition between (R1) and (R2). Whereas in the low pressure limit (R1) is the dominant loss mechanism, in the high ("infinite") pressure limit, (R2) dominates. The quantum mechanical capture probabilities we compute here are actually most directly related to this latter process and infinite pressure rate constants can therefore be estimated from them without any additional PST approximations.

The purposes of the present paper are (i) to estimate the quantum rate constant for reactions (R1) and (R2) based on extensive $J > 0$ four-atom wavepacket calculations of the capture probability and (ii) to discuss the dynamical role of

* To whom correspondence should be addressed.
† Department of Chemistry, Wayne State University.
‡ Departamento de Química Física, Universidad del País Vasco.
§ Chemical Sciences and Engineering Division, Argonne National Laboratory.

10.1021/jp805875p CCC: $40.75
Published on Web 11/14/2008

rotational excitation and alignment in determining reaction probabilities and rate constants. In order to accomplish (i), in addition to use of our previously developed QM C/PST model [Paper I], we have developed a Monte Carlo sampling procedure for selecting which reactant quantum states are considered.

Section II below outlines the theoretical methods employed, Section III presents our results, Section IV gives concluding remarks, and Appendices A and B concern details of the Monte Carlo sampling procedure and PST calculations, respectively.

II. Theory

A. Quantum Mechanical Capture/Phase Space Theory (QM C/PST) Model for Rate Constants. We begin with the standard formula for the reaction rate constant at a given temperature, T, which involves a Boltzmann distribution over the cumulative reaction probability:

$$k(T) = \frac{\sigma_{el}}{2\pi\hbar Q_r(T)} \int dE e^{-E/k_B T} N(E) \quad (1)$$

where $N(E)$ is the cumulative reaction probability, σ_{el} is an overall electronic degeneracy factor for reaction, E is the total energy of the system, and $Q_r(T)$ is the partition function of the reactants. At the energies relevant to our work, the reactants will be in their vibrational ground state so that $Q_r(T)=Q_{trans}(T)Q_{rot}(T)$. Thus, we need only consider the partition functions corresponding to relative translation and the rotational states of the diatoms. The electronic factor, σ_{el}, is taken to be $\sigma_{el} = 1/2$ to account for the fact that only one of two electronic potential energy surfaces correlates with either CH_3 of (R2) or the CH_2 + H products of (R1).[3] For a reaction of two diatomic molecules, we may rewrite the expression for the rate constant in terms of a Boltzmann-weighted average over state-specific reaction probabilities as follows:

$$k(T) = \frac{\sigma_{el}}{2\pi\hbar Q_{trans}(T)} \sum_{J=0}^{J_{max}} (2J+1) \sum_j \frac{\sigma_{nuc} e^{-E_{rot}/k_B T}}{Q_{rot}(T)} \times \int dE e^{-E_{trans}/k_B T} P^J(j,E) \quad (2)$$

In eq 2 above, $E = E_{trans} + E_{rot} + E_{vib}$. Since we consider only the vibrational ground state, $\exp(-E_{vib}/k_B T)/Q_{vib}$ is essentially unity and is thus not included.

We employ two strategies to reduce the amount of computational time required to compute the low pressure rate constants for (R1) and the high pressure rate constants for (R2). The first strategy is to approximate $P^J(j, E)$ in eq 2 with either the QM C/PST model of Paper I in the case of reaction (R1), or to simply use the quantum mechanical capture probabilities directly for $P^J(j, E)$ in the case of reaction (R2):

$$(R1): \quad P^J(j,E) = P^J_{cap}(j,E) P^J_{stat}(E) \quad (3)$$

$$(R2): \quad P^J(j,E) = P^J_{cap}(j,E) \quad (4)$$

The second strategy that we employ is to use a Monte Carlo sampling method to approximate the sums over quantum numbers given in eq 2. (See Section IIC and Appendix A). A sampling method is necessary because even though the capture probabilities are not terribly time-consuming, even at low energies, there are many thousands of possible initial states.

B. QM C/PST Probability. The method for computing the QM C/PST reaction probability is given in detail in Paper I.[3] Thus, we will give a brief description here. To compute the capture probabilities, P^J_{cap}, we employ the real wavepacket method,[18] along with a diatom + diatom Jacobi coordinates four-atom representation.[17] The wavepacket is a function of six nuclear degrees of freedom which are illustrated in Figure 1: the separation of the CH and H_2 centers of mass, R; the HH and CH internuclear distances, r_1 and r_2; and three angular coordinates θ_1, θ_2, and ϕ. We define R to be the body-fixed z axis. The angular coordinates correspond to the angles made by the HH and CH bonds with the R axis and an associated torsional angle. Evenly spaced grids are used to represent r_1 and R and the dispersion fitted finite difference (DFFD) method is used to compute the action of the kinetic energy operator.[19] Parity-adapted angular basis functions or equivalent primitive grids are used to represent the angular degrees of freedom.[17] The CH bond, r_2, is described with a potential-optimized discrete variable representation (PODVR).[20] We neglect Coriolis coupling, treating K as a good quantum number, which greatly facilitates calculations involving high J values since then K is treated as a conserved quantum number. Coriolis terms can become large when R is small since these terms are proportional to $(1/(2\mu R^2))$ and/or when large values of j_1 and j_2 are important. Because we absorb the wavepacket prior to its reaching the interaction region, neither of these conditions is met. The Boltzmann weighting of the initial rotational states does not favor large values of j_1 and j_2, and there is not much mixing of the rotational states prior to entering the interaction region. It is possible that Coriolis coupling could be somewhat important near our inner absorption region, but we do not think that inclusion of these terms would significantly alter our results.

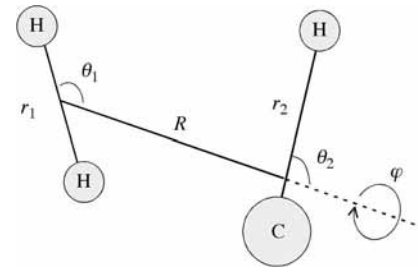

Figure 1. Schematic diagram of the four-atom Jacobi coordinates employed in our quantum calculations.

Unlike standard wavepacket calculations, our capture wavepacket calculations include absorption of the wavepacket as it enters the interaction region.[11,12] Thus, there are two absorption strips along the R grid, the usual one at the large R end for absorbing noncomplex forming CH + H_2 and one at the small R end associated with absorbing CH_3 complexes as they form in the interaction region. The absorption at small R "captures" the complex so that it cannot dissociate to form products or, more importantly, reform reactants. In preliminary testing, we found that we got very similar capture probabilities using 2 au $\leq R_{abs} \leq$ 3 au to define the absorption strip at small R. (See Table 1.) The capture probabilities are computed directly from a flux analysis. The flux is evaluated at a value of R, $R^\dagger$, that is between the inner and outer absorption regions. As long as $R^\dagger$ is not too close to the absorption region, we find that the results are independent of its exact value. For the work reported here, we set $R^\dagger$ to be 5.8 au Numerical parameters for the capture wavepacket calculations are given in Table 1. We employ the same potential energy function that was used in Paper I. [3] However, the only portion of the potential relevant to these calculations is the entrance channel. Thus, calculations of this type do not require a global potential energy surface, simply that the entrance channel be well characterized.

Sometimes probabilities can be difficult to converge at low translational energies. Due to the endothermicity of the reaction

TABLE 1: Computational Details of Capture Wavepacket Calculations

parameters (au = atomic units)	$0 \le J < 25$	$25 < J \le 32$[a]
R_{min}(au), R_{max}(au), N_R	0.5, 17.0, 216	0.5, 20.0, 255
r_{HHmin} (au), r_{HHmax} (au), N_{HH}	1.0, 6.0, 76	1.0, 6.0,48
no. of r_{CH} PODVR points	1	1
largest value of j_{HH} (j_1)	12[a],13[a]	12[a],13[a]
largest value of j_{CH} (j_2)	18	18
absorption parameters:[c] R_{abs}(au) C_{abs}(au), for R	13.5, 0.005	16.5, 0.005
absorption parameters: r_{abs}(au), C_{abs} (au) for r_{HH}	2.0, 0.005	2.0, 0.005
absorption parameters: R_{abs}(au) C_{abs}(au) for R in the interaction region	2.0, 0.1	2.0, 0.1
incoming Gaussian function:[d] $\hbar^2 k^2/(2\mu)$(eV), R_0(au), α (au)	0.3, 12.0, 0.3 (0.05, 12.0, 0.3)	0.3, 14.0, 0.3 (0.05, 14.0,0.3)
rotational constants (cm^{-1}): B_1, B_2	60.85, 14.46	60.85, 14.46
E_{vib} (eV)	0.44 eV	0.44 eV

[a] Due to symmetry, the rotational basis for H_2 contains only even or odd values of j_1. [c] The absorption is given by $\exp[-C_{abs}(R - R_{abs})^2]$, $R \ge R_{abs}$, except in the interaction region where it is applied for $R \le R_{abs}$. [d] Defined as in ref 18. For some values of the initial parameters, it was necessary to use two different initial wavepackets to cover the entire relevant spectral range. In this case, a second set of parameters was also used.

(R1), we rarely had to consider very low translational energies when finding capture probabilities relevant to the rate constants for this process. Additionally, for either (R1) or (R2), our finite T ensembles favor $J > 0$, and centrifugal barriers reduce the importance of the low translational energies. In cases where low translational energy was important, we used an additional initial wavepacket centered at low energy to better converge the capture probabilities near threshold. In a few cases, oscillations in the capture probabilities near threshold did occur, but we were able to extrapolate from slightly higher translational energies to avoid them.

The probability $P^J_{stat}(E)$ is a statistical or PST reaction probability for the complex, i.e., the ratio of the number of available product states at energy E and total angular momentum J to the total number of available reactant and product states: eq B2 of Appendix B. In subsequent equations in Appendix B, centrifugal barrier effects in the reactant and product channels are included in the available state counts. We will refer to QM C/PST calculations including such centrifugal barrier effects in the PST component as QM C/PST-1. While this QM C/PST-1 model might seem to be the most consistent one, it is possible that dynamical effects may substantially modify the effects of the barriers. One simple alternative model for $P^J_{stat}(E)$ is one that completely neglects centrifugal barrier effects in the reactant and product sum of states, i.e., effectively sets these barriers to zero. We will refer to this model as QM C/PST-2. (Note, however, that all purely PST results presented in this paper correspond to PST-1. See Appendix B.)

C. Monte Carlo Sampling Procedure. To motivate our sampling procedure, we rewrite eq 2 as follows:

$$k(T) = \frac{\sigma_{el}}{2\pi\hbar Q_{trans}} \sum_{J=0}^{J_{max}} (2J+1) \sum_j \frac{\sigma_{nuc} e^{-E_{rot}/k_B T}}{Q_{rot}} \tilde{P}^J(j,T) \quad (5)$$

where

$$\tilde{P}^J(j,T) = \int dE e^{-E_{trans}/k_B T} P^J(j,E) \quad (6)$$

is the reaction probability averaged over a Boltzmann distribution of kinetic energies.

We use a Boltzmann weighted sampling method to choose an ensemble of initial states for the wavepackets. Many of the technical details of the procedure are given in Appendix A. For ensemble state, i, with quantum numbers $J(i)$ and $j(i)$, we compute $P^{J(i)}(j(i),E)$ as defined in eq R2 and then integrate over the translational energies to obtain $\tilde{P}^{J(i)}(j(i),T)$ as defined in eq 3. For an N-member ensemble, the reaction rate is then computed as follows:

TABLE 2: Parameters Relevant to Calculations at Different Temperatures

T (K)	max E_{trans} (eV)	J_{max}
202	0.15	30
294	0.20	32
300	0.20	32
364	0.30	35
484	0.35	38
584	0.4	39

$$k(T) = \frac{\sigma_{el}}{2\pi\hbar Q_{trans}} \frac{1}{N} \sum_{i=1}^{N} \tilde{P}^{J(i)}(j(i),T)(J_{max}+1)^2 \quad (7)$$

Note that the rotational weighting factors and partition functions in eq 2 are not in eq 4 because they are accounted for in the sampling procedure. Note also that in the expression for the rate constant, eq 2, each J has a weight of $(2J + 1)$, whereas in the ensemble, eq 4, each J has a weight of $(2J + 1)/(J_{max} + 1)^2$ (see Appendix A). This gives rise to the$(J_{max} + 1)^2$ factor in eq 4, which is analogous to the b^2_{max} factor in the corresponding classical expressions for rate constants, where b_{max} is the maximum impact parameter.

III. Results and Discussion

A. Capture Probabilities. In general, the quantum mechanical capture probabilities, $P^J_{cap}(j, E)$, are complex functions of J and $j = \{K, j_1, j_2, k_1, p\}$. However, for $K > 0$, assuming that K is a good quantum number, the results are independent of parity, p. (For $K = 0$, the even and odd parity results may differ.) For given J, j_1, j_2, the quantum number, K, ranges from 0 to min $(J, j_1 + j_2)$. The allowed values of k_1 are a function of j_1, j_2 and K and in some cases may be negative.[16] In this subsection, we discuss certain trends we have found in $P^J_{cap}(j, E)$ with particular focus on the projection quantum numbers K, k_1 and $k_2 = K - k_1$ that relate to the initial orientations of the diatomics. We first present some general expectations based on the underlying potential energy surface and the nature of the initial wave functions. We move on to a discussion of a variety of capture probabilities that are consistent with these expectations. The dependence on J is also touched on at the end.

Figure 2 displays the potential surface as a function of (a) R and θ_1 and (b) R and θ_2, optimized with respect to the other coordinates. As discussed in greater detail in ref 3, the minimum

energy path for complex formation for $R > 2.5$ au corresponds to the planar configurations with the diatomics being parallel to each other and perpendicular to R, i.e., $\theta_1 = \theta_2 = 90°$ (and $\phi = 0$) in Figure 1. The more intuitive C_{2v} insertion becomes operative at $R < 2.5$ au and corresponds to $\theta_1 = 90°$ and $\theta_1 = 0°$. These features are reflected in the optimized potential plots in Figure 2.

Due to the parallel diatomic alignment preference in the entrance channel noted above, if all other things are equal, we expect that larger K quantum numbers will tend to have larger capture probabilities at the energies relevant to this study. To understand this expectation, it is important to realize that the "hidden" quantum number, $k_2 = K - k_1$, corresponds to the CH z-axis projection quantum number. The initial rotational H_2 and CH wave functions are given by a product of associated Legendre functions:

$$P_{j_1}^{k_1}(\cos\theta_1)P_{j_2}^{k_2}(\cos\theta_2) \tag{8}$$

Optimal alignment occurs when k_1 and k_2 attain their maximum values, i.e., $j_i = k_i$ because then the associated Legendre functions are proportional to $\sin^k(\theta)$ which peaks at $\theta = 90°$. The alignment is least optimal when $k_i = 0$, and becomes more optimal as k_i increases. Figure 3 illustrates this point by plotting the reduced probability density as a function of R and $\cos\theta_2$ of four different wavepackets after having been propagated a fixed time (0.05 ps) toward the interaction region. In each case, $J = 10$, $j_1 = 1$, $j_2 = 3$, and $k_1 = 1$ but K differs. (Note that the H_2 is optimally aligned.) From top to bottom, we have $K = 1$ ($k_2 = 0$), $K = 2$ ($k_2 = 1$), $K = 3$ ($k_2 = 2$), and $K = 4$ ($k_2 = 3$). As k_2 increases, there is much more density concentrated *near* $\cos\theta_2 = 0$. For the $K = 4$ case, we have $j_1 = k_1 = 1$ and $j_2 = k_2 = 3$, thus the system is optimally aligned to form CH_3 complexes (bottom panel). The least optimal alignment occurs when $K = 1$ or $k_2 = 0$, with more wavepacket density at $\cos\theta_2 = \pm 1$ (top panel).

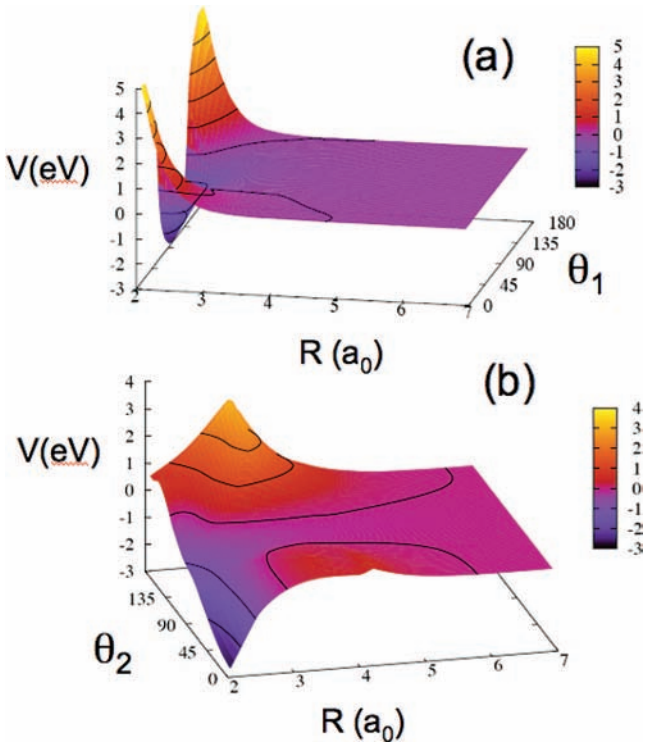

Figure 2. Optimized potential energy, V, as a function of R, the distance between the H_2 and CH centers of mass, and the angles made by the diatomics with R: (a) θ_1 (H_2), (b) θ_2 (CH).

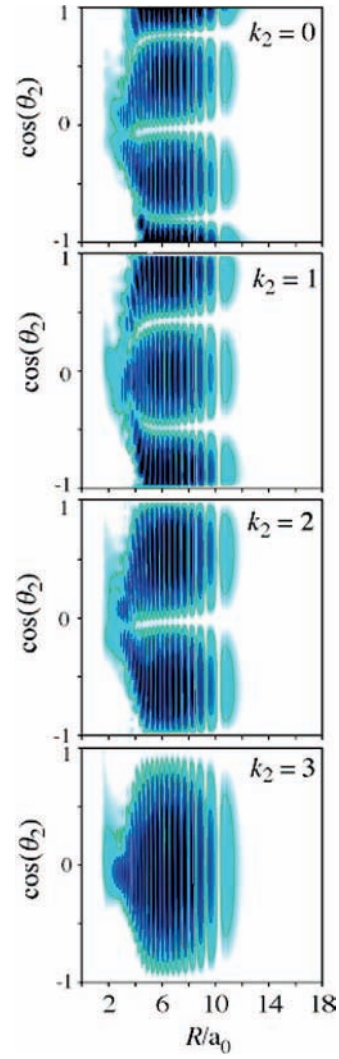

Figure 3. Snapshot of real wavepacket densities after effectively 0.05 ps of propagation from the initial condition of Table 1. In each case, the initial wavepacket had $J = 10$, $j_1 = 1$, $j_2 = 3$, and $k_1 = 1$. The K quantum number increases from 1 to 4 as one goes from top to bottom panels, which corresponds to k_2 ranging from 0 to 3 as indicated. Light blue represents low density and dark blue represents high density.

Figures 4 and 5 display $P_{cap}^J(j, E)$ results consistent with the above arguments. In each panel of Figure 4, we show $P_{cap}^J(j, E)$ for a particular choice of K (dashed curve) and $K + 1$ (solid curve) with with J, j_1, j_2, and k_1 kept the same. One sees, sometimes quite dramatically and other times less so, that the $K + 1$ capture probability is the higher one over the energy range considered. A somewhat surprising but completely consistent result with the above considerations is shown Figure 5. *If all else is equal*, then higher CH rotation reduces the capture probability. This is the case because for a fixed value of $k_2 < j_2$, increasing j_2 leads to further disparity between k_2 and j_2, and thus less optimal alignment. Each panel of Figure 5 shows that the higher j_2 case, all other quantum numbers equal, has the lower capture probability.

We have focused on the role of k_2 in this discussion, but of course, similar remarks can be made regarding k_1. However, due to the large H_2 rotational constant, the most important H_2 rotational states are relatively low so that there is not as much variation with k_1 in our ensemble.

Another important determinant of the capture probability is the total angular momentum quantum number, J. In general, all else being equal, at a given collision energy P_{cap}^J decreases

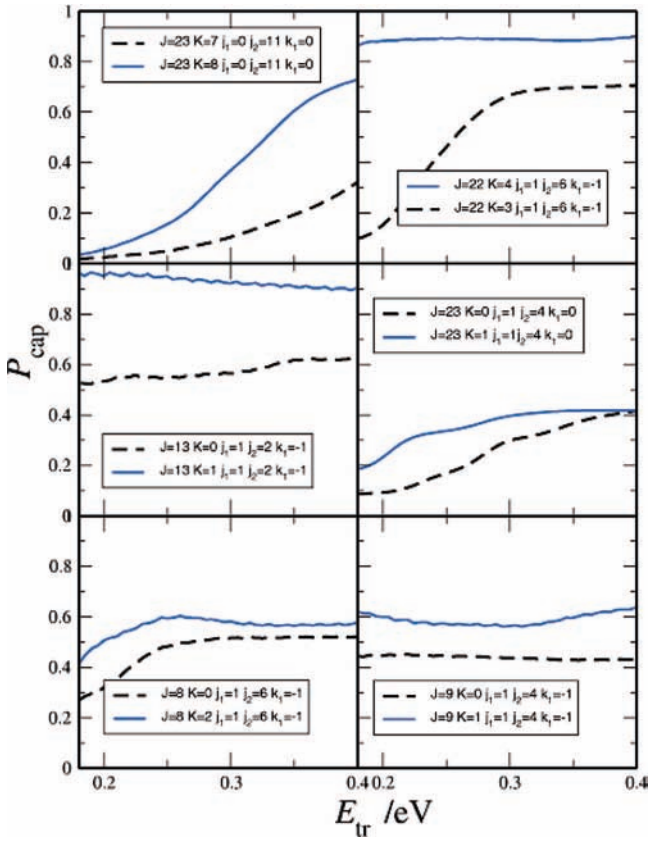

Figure 4. Capture probabilities as a function of initial translational energy. This plot shows the dependence of the capture probabilities on the projection quantum number, *K*. The initial rotational quantum numbers are given in the figure legends.

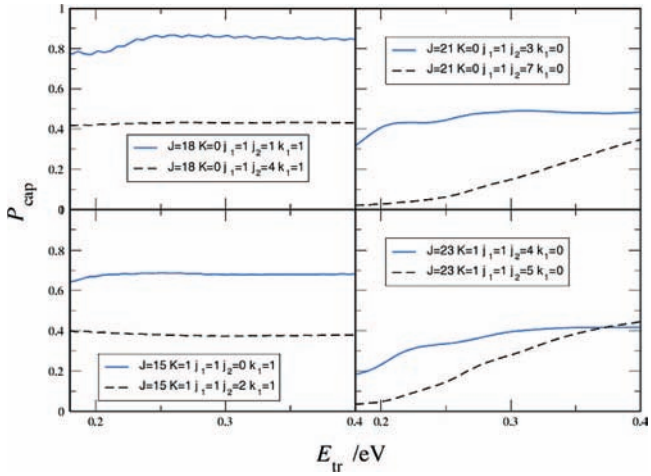

Figure 5. Capture probabilities as a function of initial translational energy. This plot shows the dependence of the capture probabilities on the j_2, the initial rotational quantum number of CH. The initial rotational quantum numbers are given in the figure legends.

with increasing *J*, as illustrated in the left-hand panel of Figure 6. This can be understood in terms centrifugal barriers in the reactant channel rising as *J* increases. For a given *J*, however, there will be very different capture profiles, depending on the values of the other rotational quantum numbers as seen in the right-hand side of Figure 6. We have used capture profiles such as those shown in Figure 6 to determine the J_{max} for each temperature.

To conclude this subsection, we note that the reactant quantum number dependence of the capture probabilities, particularly the dependence on the projection quantum numbers, implies that not all orientations have the same capture probability. Figures 4 and 5 show that this is true for reactants with the same total energy. A statistical theory based on total energy considerations and/or simple approximations to centrifugal barriers that do not depend on these projection quantum numbers, as in Appendix B, would likely overestimate the capture probabilities.

B. Rate Constants for High Pressure Collisional Stabilization, (R2). We begin with the high pressure collisional stabilization, reaction (R2), rate constants because the quantum mechanical capture probabilities alone, without additional statistical assumptions, can be used to obtain these rate constants. It is also the case that the uncertainties placed on the experimental rate constant for (R1) from ref 5 are significantly lower than those for (R1). Figure 7 presents our corresponding quantum mechanical capture (QM C) rate constants for collisional stabilization (filled circles), and contrasts those with experiment (red dashed curve) and phase space theory (PST—see Appendix B). The experimental rate constant in Figure 7 is from what Brownsford et al.[5] estimated to be their best estimate of the rate constant for reaction (R2), which was given in the form of a power law fit to their data. The solid error bars correspond to application of the 95% confidence limits to the parameters of the fit.

The QM C rate constants in Figure 7 are in good accord with experiment, whereas the PST rate constants overestimate the rate constant by about a factor of 3. This result is consistent with the dynamical effects noted in Section IIIA, i.e., the observation that orientation effects not included in PST will limit complex formation. (Of course a simple manner of determining the centrifugal barriers was used in Appendix B that ignored dependencies of these barriers on reactant quantum numbers aside from the orbital angular momentum quantum number associated with the approaching H_2 and CH fragments. More sophisticated treatments could conceivably lead to lower PST rate constants.)

C. Rate Constants for Low Pressure $CH_2 + H$ Formation, (R1). The QM C/PST rate constants, calculated using a combination of quantum mechanical capture probabilities and phase space theory, are shown in Figure 8 and compared with experimental and full classical PST results. The experimental rate constant is taken to be the best estimate of the zero-pressure (R1) rate constant from ref 5, which was given in the form of an Arrhenius fit (dashed red curve and solid error bars) in their abstract. It should be mentioned that the experimental rate constant for $T < 500$ K for R1 is not directly measured because, even at the lowest pressures in the experiment, there are contributions from both R1 and R2.[5] The error bars are inferred from the 95% confidence limits on the fit parameters. The QM C/PST-1 results (open circles), which include centrifugal barrier effects in the PST portion of the calculations, lie just at or slightly under the lower uncertainty limit of the experimentally based curve. The corresponding PST results (solid curve), which are only slightly above the experimental dashed curve, are about a factor of 3 larger than the QM C/PST-1 ones. In view of the experimental uncertainties, which are larger for (R2) than (R1), perhaps one could call the agreement between QM C/PST-1 and experiment adequate. This situation is therefore similar to the high pressure capture rate constant case of Section IIIB with the PST rate constant being larger than the QM C/PST-1.

However, if one assumes that the level of disagreement between QM C/PST-1 and experiment is significant, then there are two curious features in the results of Figure 8. First, in light

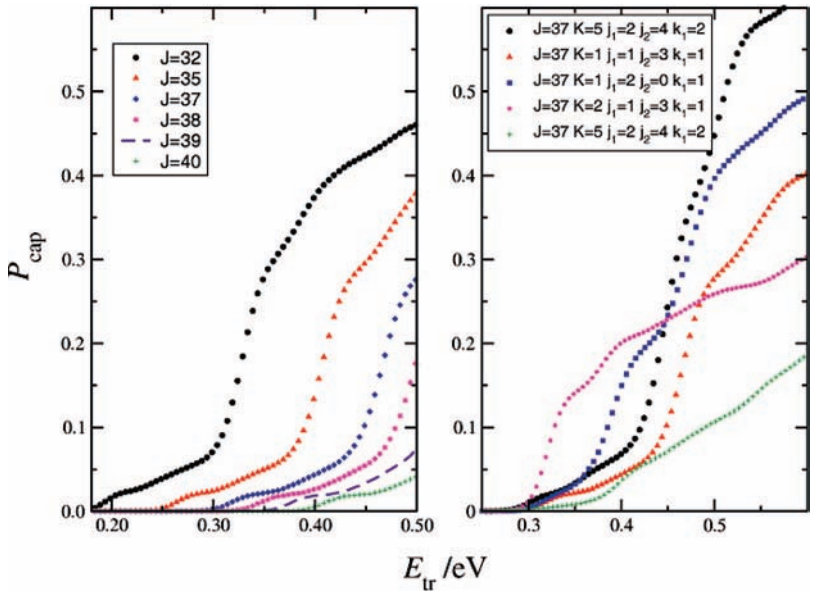

Figure 6. Capture probabilities as a function of initial translational energy. This plots shows the dependence of the capture probabilities on the overall angular momentum. On the left, all initial states have $j_1 = 1$, $j_2 = 3$, $k_1 = 1$, and $K = 1$. On the right, results for $J = 37$ from different initial conditions are presented.

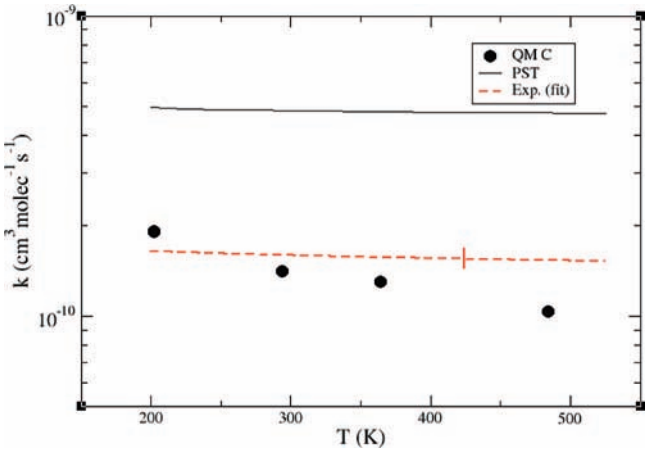

Figure 7. Infinite pressure rate constants for CH + H_2 → CH_3 inferred via the quantum mechanical capture (QM C) model, phase space theory (PST) and the experiments of ref 5. The solid vertical red line is an indication of the experimental uncertainties.

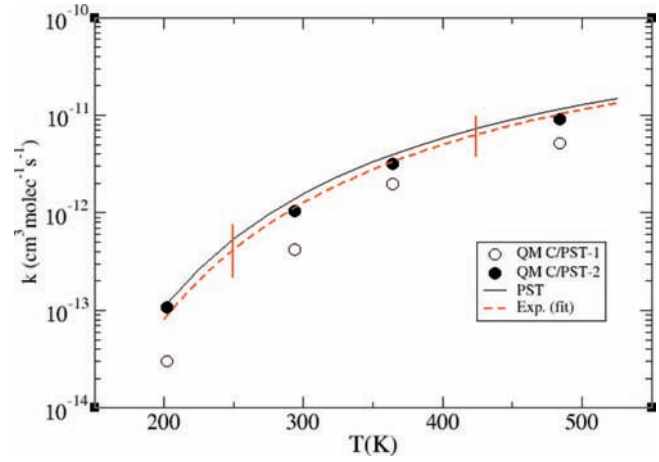

Figure 8. Low pressure rate constants for CH + H_2 → CH_2 + H inferred via the quantum mechanical capture/PST (QM C/PST-1 and QM C/PST-2) model, phase space theory (PST) and the experiments of ref 5. The solid vertical red line is an indication of the experimental uncertainties. See text for further details.

of full PST overestimating the (R2) experimental capture rate constant in Section IIIB, it is surprising that PST appears to be in much better agreement with experiment for (R1). Second, it is surprising that an approach like QM C/PST-2, that neglects centrifugal barrier effects, gives a result in better accord with experiment than QM C/PST-1, which includes these effects. Regarding the first feature, given that we know that the full PST capture probability is too high, eq R2 for (R1) implies that the only way to obtain (accidentally) a correct rate constant from PST is to then *underestimate the statistical probability of forming products once a complex has formed*. This implies that it is likely that the centrifugal barriers for product formation used in our PST calculations, relative to those for going back to reactants, are too high due to dynamical reasons yet to be determined. In other words, the correct centrifugal or dynamical barriers in the product and reactant channels that are operative may be closer to one another than expected on the basis of simple arguments. If this is the case, then one can see how the second curious feature arises. Because QM C/PST-2 uses no centrifugal barriers in the PST portion of the calculation of the calculation, it effectively lowers the relative differences between reactant and product barriers, albeit in the most extreme way. Thus, both a dynamically correct capture probability (QM C) and a possibly more correct statistical probability are being used in this case, which leads to the agreement with experiment.

IV.Concluding Remarks

We carried out calculations of the quantum mechanical capture (QM C) probabilities for CH + H_2 in six dimensions and for a variety of reactant and total angular momentum states. Rotational state dependencies in the QM C probabilities were identified which reflect orientational effects in the complex formation. We then calculated quantum-based rate constants corresponding to the infinite pressure collisional stabilization of the complexes, reaction (R2), and to the zero pressure limiting rate constant for CH_2 + H formation, reaction (R1). These results were compared with classical phase space theory (PST) results and experimental results. The rate calculations for (R1)

involved a combination of the quantum mechanical capture (QM C) probabilities and statistical or phase space theory estimates of the probability to form products.

We found very good agreement with experiment concerning our QM C rate constants for stabilization, pointing to the goodness of the potential energy surface employed and the Monte Carlo (MC) sampling procedure for evaluating the quantum rate constant. The PST rate constants are larger than the experimental and the QM C ones, consistent with the orientation effects noted in the detailed QM C probabilities. A similar but more complex picture emerged for reaction (R1). Our QM C/PST-1 rate constants for (R1), the zero pressure rate constant to form $CH_2 + H$, agree with the lower uncertainty limits of the experimental results. However, a QM C/PST calculation neglecting centrifugal barriers (QM C/PST-2) and full PST with centrifugal barriers agreed better with experiment. Assuming such differences are significant given the uncertainty in the experimental rate constant, it was argued that the effective dynamical barriers for product formation, relative to those for reactants, might be lower than those assumed in the PST calculations.

In the future, we plan to examine the quantum dynamics of product formation in more detail in order to confirm the inferences above. It would also be interesting to apply the QM C/PST method to larger systems that react via metastable intermediates. This method requires only that the full potential energy surface is known in the entrance channel. It is also quite possible that most of the vibrational degrees of freedom would not have to be treated explicitly, so that quantum wavepackets could be computed rather efficiently.

Appendix A: Monte Carlo Sampling Procedure

This Appendix discusses in greater detail the Monte Carlo approach for evaluating eq 2 which leads to the working equation, eq 4, of the text. The sampling procedure is essentially a discrete version of the standard Boltzmann weighted sampling procedure used in quasiclassical calculations of the rate constant. [21]

For each initial state, we need to choose five quantum numbers, J, j_1, j_2, K, and k_1. By allowing the projection quantum numbers K and k_1 to have both positive and negative values, we account in our ensemble for both parity states. Only in the case of $K = 0$, however, do the even and odd parity calculations give different results and actually require separate wavepacket calculations.

The first step is to choose the three quantum numbers that can be chosen independently, J, j_1, and j_2. To choose J, we choose an integer, i, at random between 1 and $(J_{max} + 1)^2$. The maximum value of the total angular momentum, J_{max}, must be obtained according to dynamical considerations and requires test calculations to determine the largest J that contributes significantly to the capture probability. For a particular i, there is just one J that satisfies:

$$J^2 < i \leq (J+1)^2 \tag{A1}$$

It is easy to see that application of this procedure results in integer J values being chosen in the range $J = 0$ to J_{max} with probability:

$$P_J = \frac{2J+1}{(J_{max}+1)^2} \tag{A2}$$

The numerator arises from the $(2J + 1)$ degeneracy factor in eq 2, which is due to M, the number of possible space-fixed z-axis projections of the total angular momentum. The denominator in eq A1 represents the total number of possible J, M quantum states if J values up to J_{max} are considered.

The maximum values of j_1 and j_2 used in the ensemble are found using the Boltzmann weighting,

$$P_{j_i}(T) = \frac{\sigma_i(2j_i+1)e^{-B_i j_i(j_i+1)/k_B T}}{Q_{rot,i}(T)} \tag{A3}$$

that determines the probability of a particular rotational state at temperature T. Nuclear spin degeneracy factors, σ_i, defined below eq R2 in the main text, are included. We choose j_{1max} and j_{2max} such that $P_{j_i}(T) > 1.0 \times 10^{-5}$. We find j_1 and j_2 with a standard Von Neuman sampling technique.[22] For each j_i, we choose an integer, j, at random between 0 and j_{imax}. To decide whether or not to include it in our ensemble, we choose a random number, r, between 0 and 1 and accept $j_i = j$ if and only if $P_{j_i}(T) \leq r$.

Once the rotational quantum numbers J, j_1, and j_2 are chosen, we must then select the remaining quantum numbers K and k_1, and p. Here, we simply enumerate all of the micro states consistent with J, j_1, and j_2, and randomly pick one of them. If the chosen state is not already a member of the ensemble, then it is added to it. The ensemble is chosen to be large enough to converge the reaction rate at the chosen temperature. In most cases, $J \geq j_1 + j_2$, and there are $(j_1 + 1)(j_2 + 1)$ possible combinations of K and k_1 or microstates. In this case, the probability of choosing a particular microstate with quantum numbers $j = \{ J, j_1, j_2, K, k_1\}$ is as follows:

$$\frac{(2J+1)}{(J_{max}+1)^2}\frac{\sigma_{nuc}\exp(-E_{rot}/k_B T)}{Q_{rot}} \tag{A4}$$

where $\sigma_{nuc} = \sigma_1\ \sigma_2$ as defined below eq 2 in the text and $Q_{rot} = Q_{rot,1}\ Q_{rot,2}$. If $J < j_1 + j_2$, there are fewer than $(j_1 + 1)(j_2 + 1)$ microstates available, so that the probability of choosing a particular microstate is somewhat larger than what would be computed for eq A3. This introduces a slight bias into our sampling which can be corrected. Wavepackets with $J < j_1 + j_2$, however, account for only 5% if the ensemble. The error introduced by this bias is typically $<\sim 1\%$, and we do not correct for it in the results reported here.

We note several subtle points, however, regarding the selection of K and k_1. By permitting both projection quantum numbers to attain both positive and negative values, we account for both parity states. In the case of $K = 0$, a negative value of k_1 is considered to correspond to odd parity. For $K \neq 0$, even and odd parity initial conditions give rise to identical results. Therefore, if our ensemble were to include both $\{J, j_1, j_2, K, k_1\}$ and $\{J, j_1, j_2, -K, -k_1\}$ we would only compute one $P_{j_i}(T)$ but count it twice. The second consideration is whether to eliminate the possibility of choosing a given set of initial conditions more than once. In the limit of very large ensembles, one would allow this possibility. Otherwise, by eliminating highly probable initial conditions from consideration, one would bias the sample in favor of less probable ones. In the limit of rather small ensembles, however, where one might want as much variety as possible, one might not allow it. In our particular case, we determined that each alternative gave rise to nearly identical results. With the above sampling procedure for the initial states, eq 2 in the text is then reduced to its Monte Carlo form, eq 5.

For each temperature examined in the text, we find that sampling typically up to 300 initial reactant states in the MC average leads to rate constants converged to within a few percent.

Appendix B: PST-Based Rate Constant

We will first outline the PST rate constant without the complication of nuclear spin degeneracies. In the final paragraph of the Appendix, we outline the changes to this approach required for including nuclear spin effects. Following ideas in refs 23−27, we approximate the rate constant for reaction (R1) as follows:

$$k_{PST}(T) = \frac{\sigma_{el}}{hQ_r}\int dE e^{-E/k_BT}\sum_J (2J+1)N^J_{react}(E)P^J_{stat}(E) \tag{B1}$$

where

$$P^J_{stat}(E) = \frac{N^J_{prod}(E)}{N^J_{react}(E)+N^J_{prod}(E)} \tag{B2}$$

and $N_{react}J$ and N^J_{prod} are reactant and product sum of states. The PST rate constant for reaction (R2) is simply the same as eq A4 but with the $P_{stat}J(E)$ factor omitted.

We take the reactant sum of states to be,

$$N^J_{react}(E) = \sum_{v_1,v_2}\sum_{j_1,j_2}\sum_j\sum_L \theta(\varepsilon_{react} - V^*_{react,L}) \tag{B3}$$

The use of a space-fixed angular momentum representation, as opposed to the body-fixed representation used in our quantum dynamics work, is more intuitive and convenient in this case. In eqs A4 and B2, the sums over total angular momentum, J, and diatomic vibrational and rotational quantum numbers, j_1 and j_2, all range from 0, 1, 2, ... The range of the j sum is determined by angular momentum addition of $\mathbf{j}_1$ and $\mathbf{j}_2$ to make j to be from $j_1 - j_2$ to $(j_1 + j_2)$. Similarly, the range of the L sum, based on adding $\mathbf{j}$ and $\mathbf{L}$ to make $\mathbf{J}$, is $J - j$ to $(J + j)$. For a given set of reactant quantum numbers, the translational energy is $\varepsilon_{react} = E - E^{rot}_{react}(j_1, j_2) - E^{vib}_{react}(v_1, v_2)$. The step function $\theta(x) = 1$, $x > 0$ and 0 otherwise ensures that the translational energy is greater than the centrifugal barrier in the reactant channel, $V^*_{react,L}$. Notice that $\theta(\varepsilon_{react} - V^*_{react,L})$ in eq B2 represents the PST approximation of the more dynamically based $P^J_{cap}(j, E)$ of the main text.

If $V_{react}(R)$ denotes the minimum energy path for complex formation starting from reactants as a function of R, the distance between the center-of-masses of CH and H_2, the reactant channel centrifugal barrier $V^*_{react,L}$ for orbital angular momentum quantum number L is the maximum of $V_{react}(R) + L(L+1)\hbar^2/(2\mu R^2)$. The minimum energy path was determined as outlined in Paper I.[3]

We take the product sum of states to be,

$$N^J_{prod}(E) = \sum_{v_1,v_2,v_3}\sum_{j_{CH_2}}\sum_{k_{CH_2}}\left(2-\delta_{k_{CH_2},0}\right)\sum_L \theta(\varepsilon_{prod} - V^*_{prod,L}) \tag{B4}$$

where $\{v_i\}$ are CH_2 vibrational quantum numbers, $j_{CH_2} = 0, 1, 2,..., k_{CH_2} = 0, 1, ..., j_{CH_2}$, and angular momentum addition of $\mathbf{j}_{CH_2}$ and $\mathbf{J}$ determines $L = j_{CH_2} - J,..., j_{CH_2} - J$. In this case, the product translational energy is determined by $\varepsilon_{prod} = E - E^{rot}_{prod}(j_{CH_2}, k_{CH_2}) - E^{vib}_{prod}(v_1, v_2, v_3)$. Note the energy scale of the product energy must be the same as that assumed for E. A prolate symmetric rotor model was assumed for the product rotational energy ($A = 73.811$ cm^{-1}, $B_{av} = 7.187$ cm^{-1}) and the vibrational energies from ref 10 were employed.

The centrifugal barriers, $V^*_{prod,L}$, in the CH_2 + H product channel were obtained by finding the maximum of $V_{prod}(\tilde{R}) + L(L+1)\hbar^2/(2\mu'\tilde{R}^2)$, where $\tilde{R}$ is the distance of H to the center of mass of CH_2 and $\mu' = m_H m_{CH_2}/(m_H + m_{CH_2})$. The potential, $V_{prod}(\tilde{R})$, is found by assuming H approaches CH_2 along the bisector of the CH_2 angle, equating the two CH bond distances, and minimizing the full potential with respect to the remaining degrees of freedom.

As noted in ref 10, the endothermicity calculated for the potential energy surface is 0.055 eV higher than an accurate experimentally based estimate. To correct for this feature we note the following:

$$\begin{aligned}\Delta H(0\text{ K}) &= E^{vib}_{prod}(0,0,0) - E^{vib}_{react}(0,0,0)\\ &= (V_{endo} + ZPE_{prod}) - ZPE_{react}\end{aligned} \tag{B5}$$

with V_{endo} being the bare potential energy difference between reactants and products and ZPE denoting zero-point energy. We use an energy scale such that the reactants' bare potential is zero, i.e., $ZPE_{react} = E^{vib}_{react}(0,0,0)$.) The product vibrational energies required in the computation of eq B2 may then be written as follows:

$$\begin{aligned}E^{vib}_{prod}(v_1', v_2', v_3') &= \Delta E(v_1', v_2', v_3') + ZPE_{prod} + V_{endo}\\ &= \Delta E(v_1', v_2', v_3') + \Delta H(0\text{ K}) + ZPE_{react}\end{aligned} \tag{B6}$$

where (B3) has been used and $\Delta E = E^{vib}_{prod}(v_1, v_2, v_3) - E^{vib}_{prod}(0,0,0)$. Use of (B6), with the ab initio values for ΔE and ZPE_{react}, but with the empirical value $\Delta H(0\text{ K}) = 0.145$ eV[3] or 3.34 kcal/mol corrects for the ab initio error in the endothermicity. Thus, an empirical correction to the endothermicity is included in all our PST calculations that involve the sum of states for products.

It is possible to incorporate tunneling into the PST calculations by replacing the step functions that enter into the state counts with tunneling probabilities as in ref 28. We have done this at the parabolic level and found that for both reactions (R1) and (R2), it has a negligible effect for the temperature range studied. This is partly due to the fact that the centrifugal barriers are relatively thick (small magnitude imaginary frequency at the barrier), which makes the tunneling probabilities for energies less than the barrier relatively small.

It is not difficult to incorporate nuclear spin effects into the approach above. We will specialize to the CH + H_2 system of interest to this work where there is a nuclear spin degeneracy factor of $\sigma_{nuc} = 1$ with j_1 = even H_2 rotational states, and $\sigma_{nuc} = 3$ for j_1 = odd states. One simply includes these factors in the rotational summations of the reactant partition function, Q_r, as well as in $N^J_{react}(E)$ of eq A4. For reasons of dynamical consistency in treating the complex decay, no such factors are included in $P^J_{stat}(E)$. (Note, for example, that CH_3 complexes formed from j_1 = even H_2 states can decay back to H_2 with j_1 = even or odd.) This type of calculation is also completely analogous to how we treat nuclear spin degeneracy in the quantum case (Appendix A). While technically we account for the nuclear spin degeneracy in this manner in all of the PST calculations we report, these effects are very small for $T \geq 200$ K and results obtained without inclusion differ at most in only the second or third significant figure.

Acknowledgment. The work at Argonne National Laboratory was supported by the U.S. Department of Energy, Office of Basic Energy Sciences, Division of Chemical Sciences, Geosciences, and Biosciences under contract DE-AC02-06CH11357. E.M.G. acknowledges support from the National Science

Foundation. A.S. is grateful for support from the Ministerio the Ciencia y Tecnologia project BQU2002-04462-C02-02. We are grateful for many helpful discussions with Drs. L. B. Harding, S. J. Klippenstein, and H. Guo. We are particularly grateful to Profs. I. W. M. Smith and I. R. Sims for advice and discussions on their experimental results.

References and Notes

(1) Brooks, B. R.; Schaefer III, F. F. *J. Chem. Phys.* **1977**, *67*, 5146.
(2) Dunning, T. H.; Harding, L. B.; Bair, R. A.; Eades, R. A.; Shepard, R. L. *J. Phys. Chem.* **1986**, *90*, 344.
(3) Mayneris, J.; Saracibar, A.; Goldfield, E. M.; Gonzalez, M.; Garcia, E.; Gray, S. K. *J. Phys. Chem. A* **2006**, *110*, 5542.
(4) Berman, M. R.; Lin, M. C. *J. Chem. Phys.* **1984**, *81*, 5743.
(5) Brownsword, R. A.; Canosa, A.; Rowe, B. R.; Sims, I. R.; Smith, I. W. M.; Stewart, D. W. A.; Symonds, A. C.; Travers, D. *J. Chem. Phys.* **1997**, *106*, 7662.
(6) Eng, R. A.; Gebert, A.; Goos, E.; Hippler, H.; Kachiani, C. *Phys. Chem. Chem. Phys.* **2001**, *3*, 2258.
(7) Goos, E.; Hippler, H.; Kachiani, C.; Svedung, H. *Phys. Chem. Chem. Phys.* **2002**, *4*, 4372.
(8) Liu, K.; Macdonald, R. G. *J. Chem. Phys.* **1988**, *89*, 4443.
(9) McIlroy, A.; Tully, F. P. *J. Chem. Phys.* **1993**, *99*, 3597.
(10) Medvedev, D. M.; Harding, L. B.; Gray, S. K. *Mol. Phys.* **2006**, *104*, 73.
(11) Lin, S. Y.; Guo, H. *J. Phys. Chem. A* **2004**, *108*, 10066.
(12) Lin, S. Y.; Guo, H. *J. Chem. Phys.* **2004**, *120*, 9907.
(13) Rackham, E. J.; Huarte-Larranaga, F.; Manolopoulos, D. E. *Chem. Phys. Lett.* **2001**, *343*, 356.
(14) Aoiz, F. J.; Gonzalez-Lezana, T.; Rabanos, V. S. *J. Chem. Phys.* **2007**, *127*, 174109.
(15) Matzkies, F.; Manthe, U. *J. Chem. Phys.* **1999**, *110*, 88.
(16) Gatti, F.; Lung, C.; Menou, M.; Chapuisat, X. *J. Chem. Phys.* **1998**, *108*, 8821.
(17) Goldfield, E. M.; Gray, S. K. *J. Chem. Phys.* **2002**, *117*, 1604.
(18) Gray, S. K.; Balint-Kurti, G. G. *J. Chem. Phys.* **1998**, *108*, 950.
(19) Gray, S. K.; Goldfield, E. M. *J. Chem. Phys.* **2001**, *115*, 8331.
(20) Echave, J.; Clary, D. C. *Chem. Phys. Lett.* **1992**, *190*, 225.
(21) Varandas, A. J. C.; Brandao, J.; Pastrana, M. R. *J. Chem. Phys.* **1992**, *96*, 5137.
(22) KalosM. H. WhitlockP. A. *Monte Carlo Methods*; John Wiley & Sons: New York; 1986.
(23) Light, J. C. *J. Chem. Phys.* **1964**, *40*, 3221.
(24) Pechukas, P.; Light, J. C. *J. Chem. Phys.* **1965**, *42*, 3281.
(25) Lin, J.; Light, J. C. *J. Chem. Phys.* **1966**, *45*, 2545.
(26) Light, J. C. *Disc. Faraday Soc.* **1967**, *44*, 14.
(27) Gross, A.; Mikkelsen, K. V.; Stockwell, W. R. *Int. J. Quantum Chem.* **2001**, *84*, 479.
(28) Miller, W. H. *J. Am. Chem. Soc.* **1979**, *101*, 6810.

JP805875P